

The STAR Photon Multiplicity Detector

M. M. Aggarwal^a, S. K. Badyal^b, P. Bhaskar^c, V. S. Bhatia^a,
 S. Chattopadhyay^c, S. Das^c, R. Datta^b, A. K. Dubey^d,
 M. R. Dutta Majumdar^c, M. S. Ganti^c, P. Ghosh^c, A. Gupta^b,
 M. Gupta^b, R. Gupta^b, I. Kaur^a, A. Kumar^a, S. Mahajan^b,
 D. P. Mahapatra^d, L. K. Mangotra^b, D. Mishra^d,
 B. Mohanty^d, S. K. Nayak^b, T. K. Nayak^c, S. K. Pal^c,
 S. C. Phatak^d, B. V. K. S. Potukuchi^b, R. Raniwala^e,
 S. Raniwala^e, R. Sahoo^d, A. Sharma^b, R. N. Singaraju^c,
 G. Sood^a, M. D. Trivedi^c, R. Varma^f, Y. P. Viyogi^c

^a*Physics Department, Panjab University, Chandigarh 160014, India*

^b*Physics Department, Jammu University, Jammu 180001, India*

^c*Variable Energy Cyclotron Centre, Kolkata 700 064, India*

^d*Institute of Physics, Bhubaneswar 751005, India*

^e*Physics Department, Rajasthan University, Jaipur 302004, India*

^f*Indian Institute of Technology, Mumbai 400076, India*

Abstract

Details concerning the design, fabrication and performance of STAR Photon Multiplicity Detector (PMD) are presented. The PMD will cover the forward region, within the pseudorapidity range 2.3–3.5, behind the forward time projection chamber. It will measure the spatial distribution of photons in order to study collective flow, fluctuation and chiral symmetry restoration.

1 Introduction

A preshower Photon Multiplicity Detector (PMD) will be installed on the east wall of the wide angle hall in 2002 shutdown period in STAR. This detector is designed to measure photon multiplicity in the forward region where high particle density precludes the use of a calorimeter. Fig 1 shows the PMD relative to other detectors within the STAR setup as implemented through GEANT simulation. The inclusion of the PMD enhances the phase space coverage of

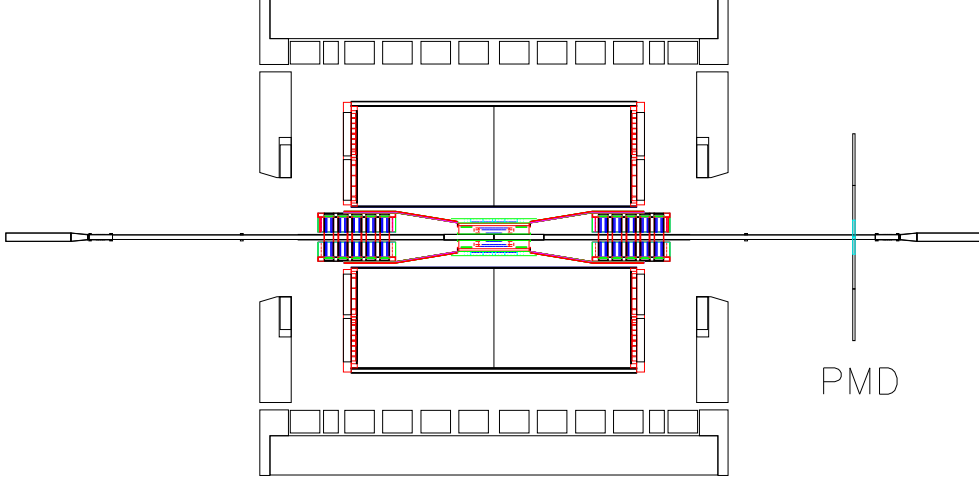


Fig. 1. The PMD in the STAR set up relative to central detector TPC. The PMD is located at 550 cm from vertex and kept outside the STAR magnet.

STAR with photons considerably, in pseudorapidity ($\eta = -\ln \tan\theta/2$) upto $\eta = 3.5$ with full azimuthal acceptance and in p_T down to about 25 MeV/c [1,2].

Using the measurement of multiplicity and spatial distribution of photons on an event by event basis and combining the information from other detectors, the PMD will be able to address the following broad topics in physics : (a) determination of reaction plane and the probes of thermalisation via studies of azimuthal anisotropy and flow, (b) critical phenomena near the phase boundary leading to fluctuations in global observables like multiplicity and pseudorapidity distributions, and (c) signals of chiral symmetry restoration (e.g., disoriented chiral condensates).

The basic principle of the measurement of photon multiplicity using the PMD is similar to those of preshower detectors used in WA93 and WA98 experiments at CERN SPS [3,4]. It consists of highly segmented detector placed behind a lead converter of suitable thickness. A photon produces an electromagnetic shower on passing through the converter. These shower particles produce signals in several cells of the sensitive volume of the detector. Charged hadrons usually affect only one cell and produce a signal resembling those of Minimum Ionizing Particles (MIPs). The thickness of the converter is optimized such that the conversion probability of photons is high and transverse shower spread is small to minimize shower overlap in a high multiplicity environment. In order to have better hadron rejection capability, another plane of the detector of identical dimension as of the preshower part is placed before the lead plate, which acts as a veto for charged particles.

The detector is based on a proportional counter design using Ar + CO₂ gas mixture. This gas mixture is preferred because of its insensitivity to neu-

trons. To handle the high particle density in the forward region, the detector technology has been chosen with the considerations that (i) multihit probability should be less (ii) MIP should be contained in one cell, (iii) low energy δ -electrons should be prevented from travelling to nearby cells and causing cross-talk among adjacent cells. Requirement of granularity and isolation of cells require the segmentation of the detector gas volume with material effective for reducing δ -electrons from crossing one cell to other. We have used honeycomb cellular geometry with wire readout. The copper honeycomb body forms the common cathode and is kept at a large negative potential. It also supports the printed circuit boards (PCBs) which are used for signal collection and for extension of the cathode required for proper field shaping. Details can be found in [5,2].

The present article is organised as follows. The detector hardware and support structure are described in Section 2. The front-end electronics and readout scheme are described in Section 3. Performance of the prototypes and a comparison with simulation results are described in Section 4. A summary is presented in Section 5.

2 The Detector

The detector consists of an array of hexagonal cells. A unit cell is shown schematically in Fig. 2(a) along with a longitudinal section illustrating the use of extended cathode for field shaping. This design was arrived at after several simulation studies and prototype tests and ensures uniform charged particle detection efficiency throughout the cell [6].

A honeycomb of 24×24 cells forms a unit module. This is a rhombus of side approx. 254 mm having identical boundaries on all the four sides. Cell walls at the boundary are kept half as thick as those inside so that adjacent unit modules join seamlessly.

A set of unit modules are enclosed in a gas-tight chamber called supermodules. The number of unit modules varies from 4 to 9 within a supermodule. The STAR PMD consists of 24 supermodules arranged in the form of a hexagon as shown in Fig. 2(b). This geometry ensures full azimuthal coverage with minimum number of supermodules.

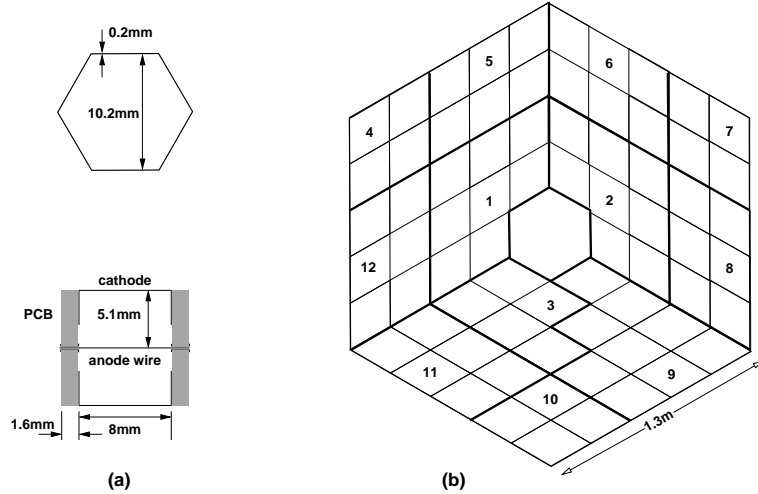


Fig. 2. (a) Unit cell schematic with cross-section showing the dimensions and the cathode extension, (b) Layout of the STAR PMD. Thick lines indicate supermodule boundaries. There are 12 supermodules each in the preshower plane and the veto plane. Divisions within a supermodule denote unit modules.

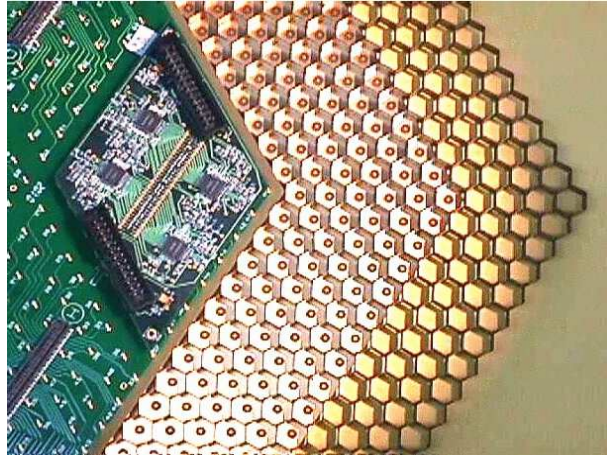


Fig. 3. Components of a unit module : Copper honeycomb, placed between two PCBs. The top PCB is seen with connectors and a FEE board. The cathode extension on the inside of the bottom PCB and the island separating the anode wire with the cathode is visible through the honeycomb. The photograph was taken with unassembled components.

2.1 Unit Module

The components of a unit module are shown in Fig. 3. It consists of a custom-built copper honeycomb sandwiched between two PCBs which hold the anode wire and provide extension to cathode. The top PCB, containing the electronics boards, has solder-islands at the centre of each cell with a 0.5 mm dia gold-plated through-hole. Signal tracks from cluster of 64 cells are brought to a 70-pin connector. The PCBs on the bottom side have only soldering islands

without signal tracks, serving as anchor points. The inner part of the PCBs are gold-plated, with circular islands near the anode wire and form part of the extended cathode.

A copper unit cell is the building block of the honeycomb. It is fabricated using 0.2 mm thick ETP grade copper sheets which are solder-coated on one side. The sheet is cut to precise dimensions along with notches and bent in hexagonal form with precision dies. These are arranged in a 24×24 matrix in a high precision jig of rhombus shape. Hexagonal Stainless Steel inserts, having dimensions matching the inner dimensions of the cell, are inserted in each cell. The assembly is heated so that soldered surfaces join to form a rigid honeycomb.

The honeycomb, after cleaning, is dip-coated with high conductivity graphite paint having thickness of $\sim 10 \mu\text{m}$. The unit honeycomb module has stiff 1 mm dia. brass screws situated at 24 different locations, which act as guides for attaching the PCBs on both sides, ensuring proper alignment. They are also used to bring out the high voltage connections of the cathode onto the PCBs. The two PCBs are attached on both sides of the honeycomb, aligning with the screws. These screws protrude only 0.5 mm above the PCB surface and are fixed with thin nuts on the surrounding islands. The islands are covered with ABS plastic caps.

The gold-plated tungsten wires ($20 \mu\text{m}$ dia.) are inserted through the holes on the PCBs, using a needle and a tensioning jig. After applying tension of $\sim 30\%$ of the elastic limit, the wires are soldered onto the islands on the PCBs about 3 mm away from the hole (for details see Ref. [5]). The plated through-holes, where wires emerge, are then closed with a tiny amount of fast-setting epoxy to make them gas-tight. This scheme prevents creepage of solder flux into the cell and makes soldering easier.

A moulded FR4 edge frame is bonded to the top PCB. This frame has a beveled outer wall which forms a V-shaped groove between the boundaries of the adjoining unit modules.

Quality assessment for the fabrication of the unit module is done by several ways, viz, visual inspection of the solder joints and epoxy filling in the holes and measurement of resistance of each wire to monitor dry-soldering contacts. Resistance measurement shows that the RMS is within 5% for one unit module. In addition, high voltage tests are also performed after connecting the front-end electronics boards and the pedestals of chips monitored to test stable operation of the detector.

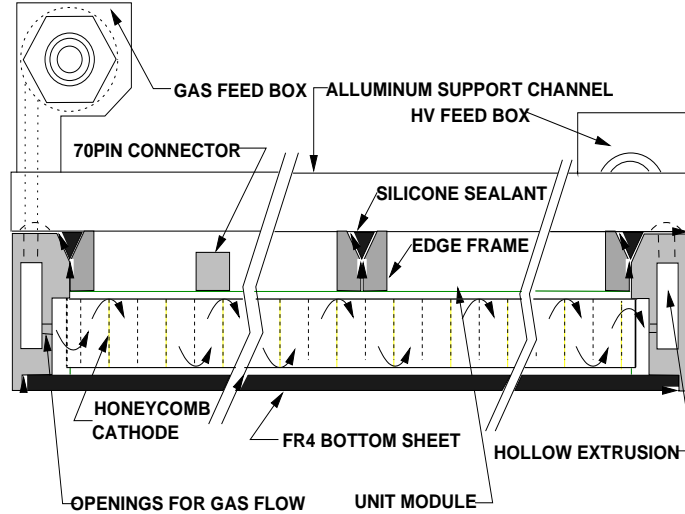


Fig. 4. Schematic cross-section of a supermodule showing the boundary walls, gas flow channels, high voltage connection and gas-tight sealings.

2.2 Supermodule

Supermodule is a gas-tight chamber made of 3 mm thick FR4 grade glass epoxy sheet as the base plate and a 7 mm thick and 25 mm high aluminum boundary wall. A schematic cross-section of a supermodule is shown in Fig. 4. The opposite sides of the boundary walls have gas-feed channels. Each channel has 24 openings into the chamber. This scheme, along with the notches in the cells, keep the gas flow impedance low. A set of assembled unit modules are placed to fill the inner area of the supermodule enclosure, leaving a gap of 1 mm on all sides to accommodate general assembly tolerance and to provide insulation between the honeycomb cathode and the boundary. Teflon spacers are inserted into this gap all along the boundary to arrest any movement of the unit modules and also to insulate the honeycomb cathode from the walls. The groove formed at the junctions of all the unit modules and between the boundary walls and the unit modules are filled with high viscosity silicone adhesive compound to make the chamber gas-tight.

Gas is fed through the connector at the end of the long gas feed channel. It enters through all the entry points in the channel simultaneously, at the depth of 4 mm from the bottom of the chamber. It then flows through the notches and exits at the other edge of the supermodule through the 24 openings of the output channel. An aluminum enclosure containing one SHV connector, an HV limiting resistor and decoupling capacitor is now fixed at one corner of the supermodule very close to the HV tapping point.

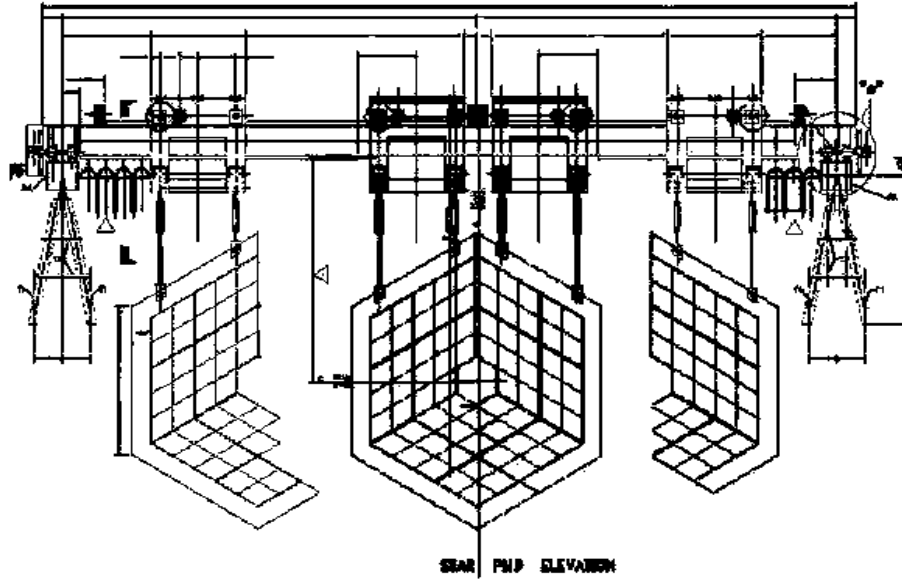


Fig. 5. PMD support mechanism. The inner hexagonal part shows the two halves joined during data taking operation. The two halves, when separated for servicing, look as shown on the right and left.

2.3 Support Structure

The drawing of the support structure is shown in Fig. 5. It has two parts: (a) the support plates, and (b) the suspension movement mechanisms. A 5 mm thick flat stainless steel plate is used to support the lead converter plates and supermodules in each half of the PMD. It has tapped holes for screws corresponding to hole positions in the lead plates and in the supermodules. The lead converter plates are sandwiched between two layers of gas detectors.

The two halves of the detector are supported on the girders and hang freely in a vertical position. The support structure allows both x - and z - movements of the detector. Each half of the detector can be separated for access by a smooth independent movement controlled by limit switches. The hanging elements have free swinging pivots, fine adjustments for horizontal motion, and plane position adjustments for alignment of the detector. The services of the two halves are also independent. When fully open, the two halves provide sufficient clearance for the poletip support of the STAR magnet to move in.

The edges of the support plate are also used for mounting the gas feed manifolds, show boxes for low voltages supplies and general support for distribution of cables onto the detector.

3 The Front End Electronics and Readout

The front-end electronics for processing the PMD signals is based on the use of 16-channel GASSIPLEX chips developed at CERN [7] which provide analog multiplexed signals and readout using the custom built ADC board (C-RAMS)¹. C-RAMS can handle a maximum of 2000 multiplexed signals. Considering the symmetry requirements of the detector hardware, the readout of the entire PMD has been divided into 48 chains. Each chain covers three unit modules and has 1728 channels.

Each readout chain is driven by (i) a translator board (ii) 27 FEE boards each consisting of 4 GASSIPLEX chips and (iii) a buffer amplifier board.

(i) Translator Board: It converts NIM levels of all control signals into the level required for the operation of GASSIPLEX chips. Operating voltage for these chips is $\pm 2.75\text{V}$ and hence all the NIM signals are to be translated to 0 to 2.75 V levels.

(ii) FEE board: The cells in the unit modules are arranged in clusters consisting of 8×8 cells connected to a 70-pin connector. This cluster of 64 cells is read out by a FEE having four GASSIPLEX chips. One such board is shown in Fig. 6. For geometrical considerations the FEE board is also made in rhombus shape. When all the boards are placed on the detector, they almost fully cover the detector area. This arrangement helps to reduce the material and also provides a ground shield for the detector.

To reduce voltage drops over a long chain of 1728 channels, a bus-bar like design has been adopted to provide power to the FEE boards. To protect the input channels against high voltage spikes, a provision has been made on the board layout to connect a diode protection circuit.

(iii) Buffer amplifier board: The buffer amplifier is used for the transmission of a train of analog multiplexed signals to the readout module via a low impedance cable.

Digitization using C-RAMS requires that all multiplexed pulses within a chain should have the same polarity. In order to read the full chain, the pedestals in the chain need to be adjusted to the minimum of the pedestals in the chain. This shifting of the pedestal effectively reduces the dynamic range. To minimize the reduction in dynamic range due to pedestal adjustment, we need to select the chips for a chain having minimum pedestals in very close range.

For proper quality control in the assembly of FEE boards, each GASSIPLEX

¹ Obtained from CAEN, Italy

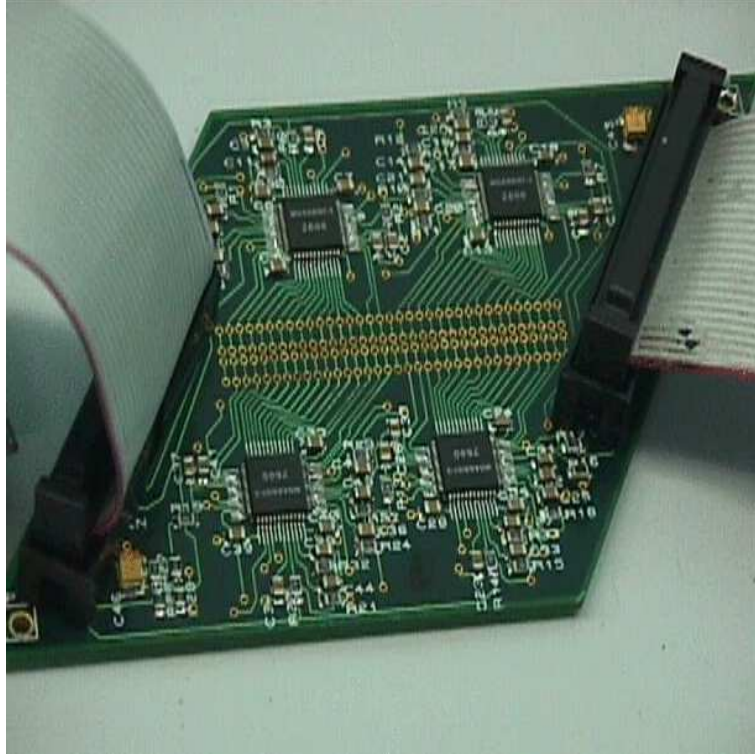


Fig. 6. Photograph of a FEE board with four GASSIPLEX chips.

chip has been tested for full functionality of each channel. In addition the pedestals of all the channels have been measured. The minimum pedestal as well as the spread in pedestal has been determined for each chip.

Fig. 7 shows (a) the distribution of pedestal minima and (b) scatter plot of pedestal minima vs. pedestal spread for 5000 chips. It is seen that we can select chips of four categories having close ranges of pedestal minima and pedestal spreads. The narrow width of the distribution shows that the usable number of chips is a large fraction of the total number of chips tested.

4 Performance of the PMD

Detailed tests have been performed with the prototype detector using pion beam at the CERN PS for the study of the response of the minimum ionizing particle (MIP) and electron beam with lead converter for estimating the performance of the preshower characteristics of the detector. Operating parameters, e.g., the composition of the gas mixture and applied HV have been optimized by these tests. GEANT simulation has been performed to study the effect of upstream material on the physics performance of the PMD. We discuss here some of the results.

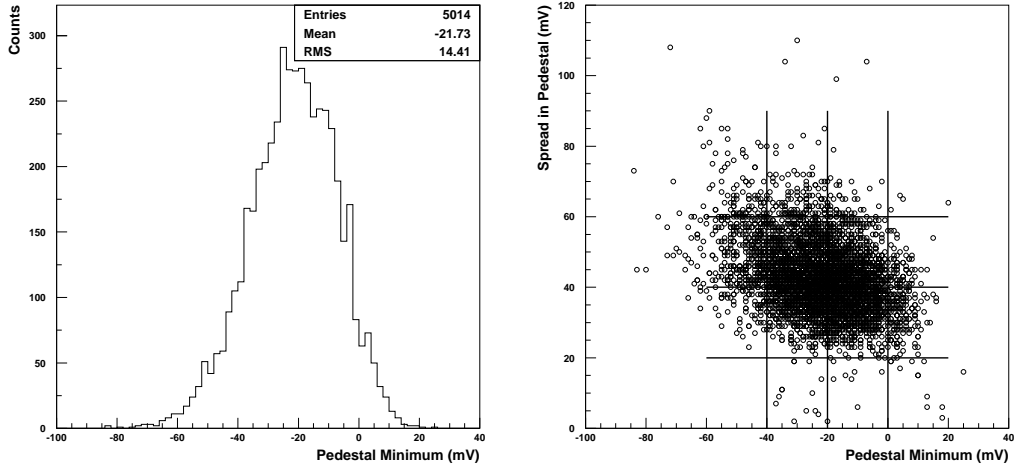


Fig. 7. (a) Pedestal minimum values (in mV) for 5000 chips, (b) pedestal minimum vs. pedestal spread for these chips. Lines are drawn to suggest the grouping of chips for a uniform chain.

4.1 Response to charged particles

Fig. 8(left) shows a typical MIP pulse height spectrum with applied voltage of -1500 V. Fig. 8(right) shows the number of cells hit by MIP, which is close to one. This suggests that charged hadron signal is essentially confined to one cell and satisfies one of the main design criterion of the detector.

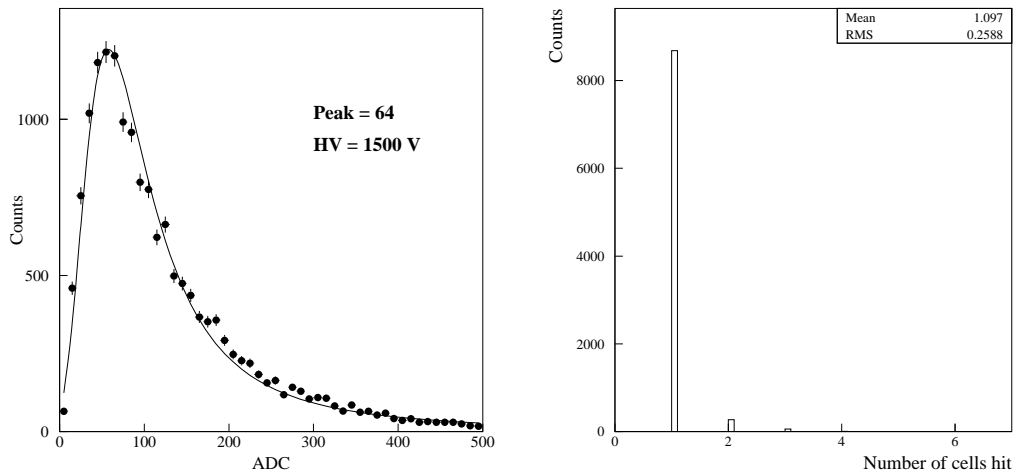


Fig. 8. (left) Typical MIP spectra for cells with -1500V , (right) Distribution of the number of cells hit by MIP, it is seen that MIP is contained mostly in one cell.

The efficiency for charged particle detection and the gain of the cell has been determined for a number of cells chosen randomly in the prototype. Fig. 9 (top) shows the histogram of the relative gains of 40 cells. The relative gain is

defined by the ratio of the mean pulse height in a cell to the average value of the mean pulse heights of all the 40 cells taken together. The overall gain of the prototype chamber is found to be quite uniform, the distribution having a narrow width of $\sigma \approx 6\%$. Fig. 9(bottom) shows the efficiency for 40 cells. The average value of the efficiency is found to be 98%. The efficiency is also uniform over the cross-section of the hexagon within a single cell, varying within a narrow range of 93–99%. the lower value being at the edges of the cell.

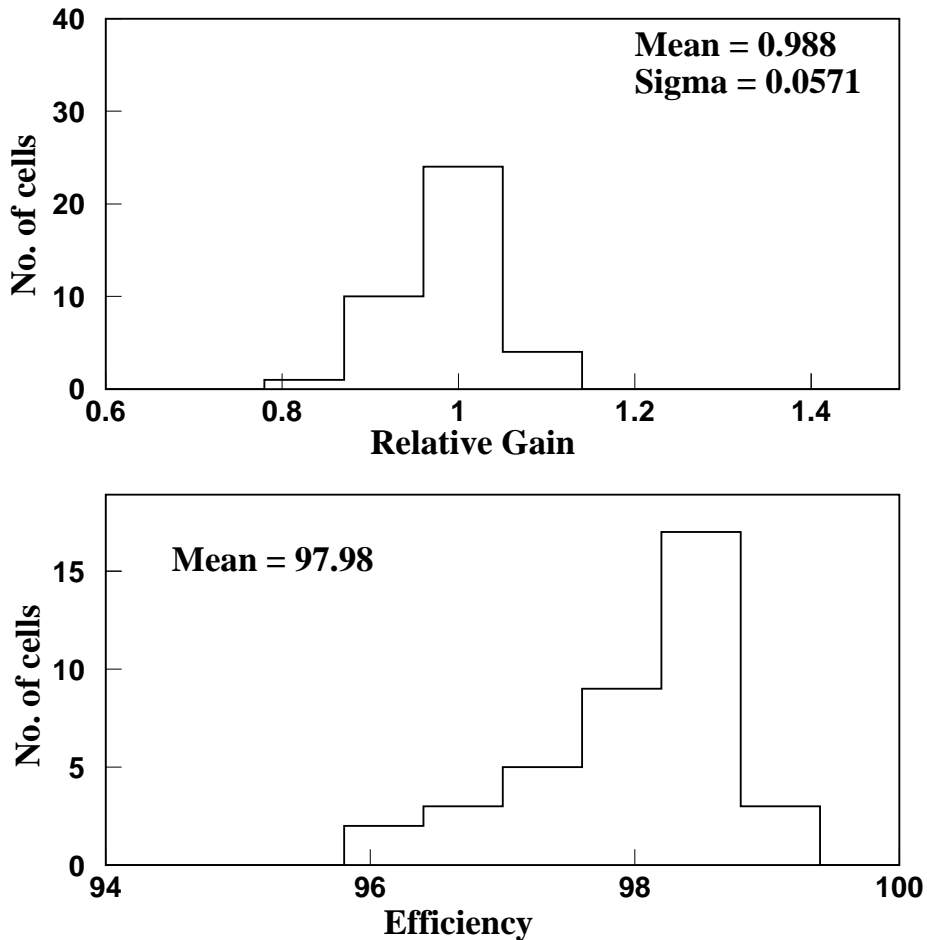


Fig. 9. Distributions of (top) gain and (bottom) efficiency for randomly selected 40 cells from the prototype chamber.

4.2 Preshower Characteristics

Preshower behaviour is characterised by (a) the transverse spread of the shower, which is given by the size of the cluster of hit cells, and (b) by the

energy deposition expressed in terms of the cluster signal (i.e., the total signal in all the hit cells, in ADC units). These have been determined using 1–6 GeV electrons and a $3X_0$ thick lead converter kept in front of the prototype detector.

The typical preshower spread for 3 GeV electrons is shown in Fig. 10 (left). Cluster size obtained from test data is very close to the values obtained from GEANT simulation, thereby suggesting that the occupancy of the detector for a given multiplicity can be obtained reliably with GEANT simulation.

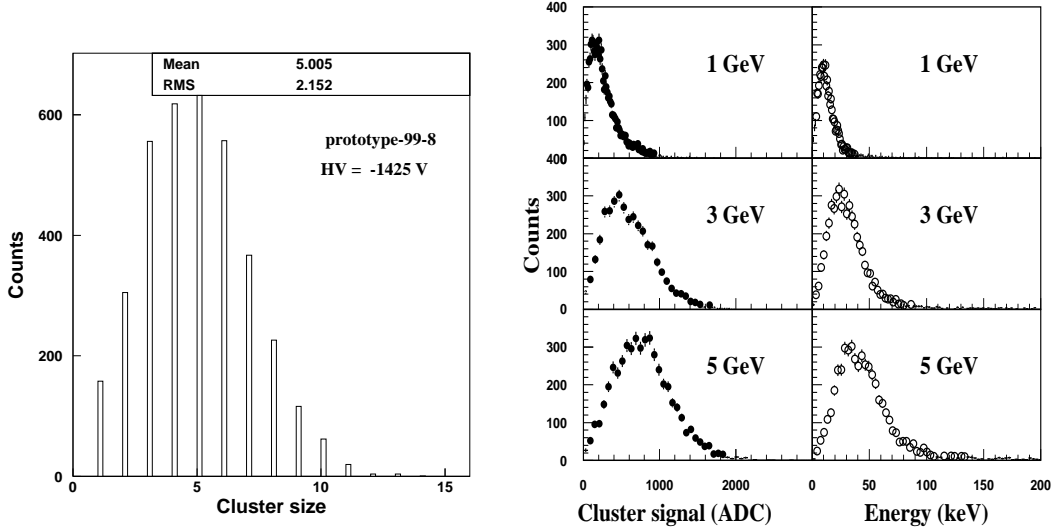


Fig. 10. (left) Typical cluster size for preshower expressed in terms of the cells affected by electron, (right panel, filled circle) energy deposition (in terms of cluster ADC) spectra for electrons with 3 different energies, (right panel, open circle) Simulated energy deposition (in keV) for electrons with corresponding energies. Width of simulated spectra is smaller compared to test data.

4.3 Simulation of the preshower response of the detector

The energy deposition spectra for electrons at various energies as obtained from test data and those obtained from the GEANT simulation at corresponding energies are shown in Fig. 10(right panel). Even though the shapes look similar, the relative widths in the preshower spectra are larger for test data compared to those in simulation. This difference is due to fluctuations in gas ionization, signal generation and transmission process in data, which are not accounted for in simulation. It was therefore necessary to estimate and introduce this difference in widths with proper modeling. We refer this addition in spread to the simulated spectra as *readout width*.

Fig. 11 (left) shows the readout width for a range of energy deposition values. For this plot, data using $2 X_0$ thick converter have also been used. From the

given plot, we can deduce the readout width for any given energy deposition obtained from GEANT simulation and fold the values for detailed comparison with experimental data.

Fig. 11 (right) shows the mean energy deposition obtained from simulation plotted against the mean ADC obtained for a particle of given energy. The response of the detector and readout is seen to be fairly linear in the range of energy studied, upto that expected from 10 GeV photons in the preshower part.

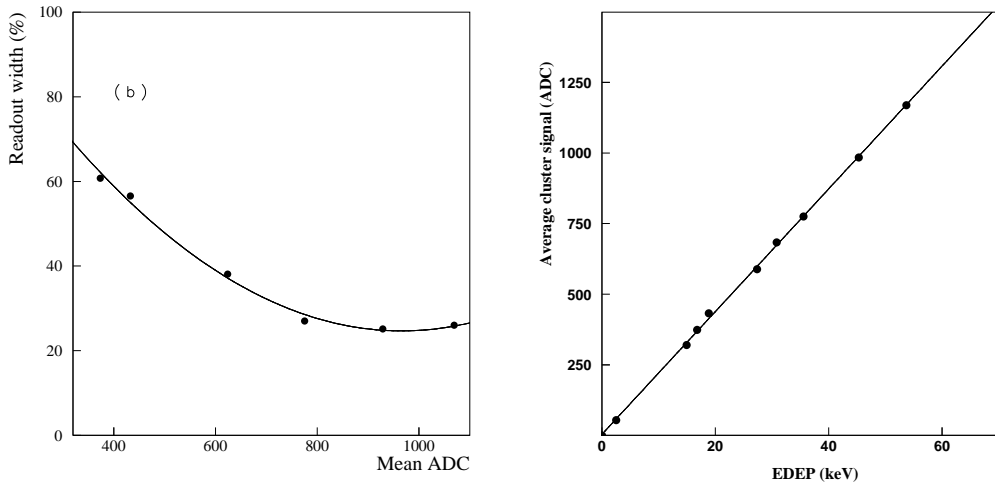


Fig. 11. (left) Readout width (%) shown for various energy deposition expressed in terms of cluster ADC, (right) Calibration plot, showing the relation between the energy deposition obtained from simulation and the cluster ADC obtained from test data.

4.4 Photon counting efficiency

For counting of photons using the preshower PMD, clusters of hit cells are determined and then a suitable algorithm is used for discrimination of charged hadrons giving signal on the preshower plane. Usually a small percentage of charged hadron signals pass the discrimination test and mix with the photon sample, causing the purity of the sample to decrease. Due to the presence of upstream material from other STAR detectors, a part of photons may get converted and fall on the PMD as charged particles. In addition high particle density causes overlap of clusters and reduces the number of good photon clusters.

The physics performance of the preshower PMD is characterized by two quantities : photon counting efficiency (ϵ_γ) and purity (f_p) defined by the following relations [4]:

$$\epsilon_\gamma = N_{\text{cls}}^{\gamma,\text{th}} / N_{\text{inc}}^\gamma , \quad (1)$$

$$f_p = N_{\text{cls}}^{\gamma,\text{th}} / N_{\gamma\text{-like}} . \quad (2)$$

where N_{inc}^γ is the number of incident photons from the event generator, $N_{\text{cls}}^{\gamma,\text{th}}$ is the number of photon clusters above the hadron rejection threshold and $N_{\gamma\text{-like}}$ is the total number of clusters above the hadron rejection threshold. $(1-f_p)$ is the fractional contamination in the $N_{\gamma\text{-like}}$ sample.

Using GEANT simulation and an event generator, the photon counting efficiency and purity for the PMD have been studied in the actual environment of STAR experiment. For the present case, both the efficiency and purity are found to be around 60%.

5 Summary

The preshower PMD, based on honeycomb proportional counter design, will be an important addition to the STAR experiment. The detector consists of two identical planes of high granularity, one placed in front of lead converter and acting as charged particle veto, and another behind the converter acting as preshower detector. Each plane has 12 supermodules, a supermodule being a gas-tight chamber consisting of 4 to 9 unit modules of 576 cells arranged in a rhombus matrix.

Prototypes have been tested to study charged particle detection and preshower characteristics. The performance satisfies the main design criteria quite well. The cellular design is found to contain δ -electrons and minimize the spread of the signal to neighboring cells. The charged particle signal is confined mostly to one cell. With the inclusion of extended cathode geometry, the efficiency is quite uniform over the entire cell.

The preshower data show that the transverse shower size is in close agreement with single particle GEANT simulations. Average pulse height of the preshower follows a linear relation with energy deposition for a wide range, upto that expected from 10 GeV photons in the preshower part of the STAR PMD.

The fabrication procedure for unit modules and supermodules incorporate quality control measures to guarantee the performance of the whole detector as observed for the prototype.

The front-end electronics is based on the 16-channel analogue multiplexed GASSIPLEX chips for signal processing and C-RAMS ADCs for readout. There are 48 readout chains, each having 1728 channels. FEE boards containing four GASSIPLEX chips have been designed to allow modularity. Chips within a chain are selected, after functionality and pedestal tests, to have close values of pedestal minima.

The PMD, covering the pseudorapidity region $2.3 \leq \eta \leq 3.5$ with full azimuthal acceptance and placed behind the FTPC, will be used to study fluctuation, flow and chiral symmetry restoration. It will measure the spatial distribution of photons with an efficiency of about 60% and a purity of about 60%.

Acknowledgements

We wish to express our gratitude to the Department of Atomic Energy and the Department of Science and Technology of the Government of India for their support in this project. One of us (SD) acknowledges the grant of research fellowship of the Council of Scientific and Industrial Research in India. Permission by CERN to allow the use of GASSIPLEX chips is gratefully acknowledged. The R&D for the detector was carried out as a joint program with ALICE PMD at CERN and the test beam facilities of CERN have been used extensively. The support of CERN staff for test beam is acknowledged. We are specially thankful to J.C. Santiard for help in the development of front-end electronics and readout scheme.

References

- [1] “A Preshower PMD for STAR Experiment”, STAR Note 310 (1997).
- [2] “Photon Multiplicity Detector for STAR : Technical Proposal”, VECC Internal Report VECC/EQG/00-04, May 2000, revised : Jan. 2001.
- [3] M.M. Aggarwal et al., Nucl. Instr. Meth. A372 (1996) 143.
- [4] M.M. Aggarwal et al., Nucl. Instr. Meth. A421 (1999) 558.
- [5] ALICE PMD Technical Design Report, CERN/LHCC 99-32 (1999).
- [6] M.M. Aggarwal et al., Nucl. Instr. Meth. sec. A, (in press), nucl-ex/0112016.
- [7] ALICE HMPID Technical Design Report, CERN/LHCC 98-19 (1998).